Organic & Biomolecular Chemistry

Cite this: *Org. Biomol. Chem.*, 2012, **10**, 2380

www.rsc.org/obc

COMMUNICATION

# A highly selective and sensitive *in vivo* fluorosensor for zinc(II) without cytotoxicity†

**Tarun Mistri,[a] Malay Dolai,[a] Debrup Chakraborty,[b] Anisur Rahman Khuda-Bukhsh,[b] Kalyan Kumar Das[a] and Mahammad Ali*[a]**

*Received 13th December 2011, Accepted 16th January 2012*
**DOI: 10.1039/c2ob07084g**



**A highly selective and sensitive fluorescent $Zn^{2+}$ sensor, 2,6-bis(2-hydroxy-benzoic acid hydrazide)-4-methylphenol (1), was designed and synthesized. In aqueous THF (4 : 6 v/v) ligand 1 induces a 2 : 1 complex formation with respect to $Zn^{2+}$ at physiological pH. This probe features visible light excitation(390 nm) and emission (490 nm) profiles, excellent selectivity responses for $Zn^{2+}$over other competing biological metal ions with $K_d < 1$ pM$^2$, LOD < 1 ng L$^{-1}$ and about 680 fold enhancement in fluorescent intensity upon $Zn^{2+}$ binding. It also exhibits cell permeability and intracellular $Zn^{2+}$ sensing in A375 human melanoma cancer cell.**

Zinc is the second most abundant transition metal in our body after iron and it is essential for normal cellular functions leading to normal human growth and development. It also serves an additional signalling role in the Central Nervous System (CNS),[1] which contains high levels of $Zn^{2+}$,[2] largely localized into the synaptic vesicles of excitatory nerve terminals.[3] The behavior of several ion channels and receptors,[4] like NMDA and potentiation of AMPA receptors[5] are affected on the release of $Zn^{2+}$ from nerve terminals after transient global ischemia[6] sustained seizures,[7] and head trauma.[8] However, little is known about the distribution, accumulation and mobility of intracellular zinc. The major challenge is to apply a Zn-sensor to real-life situations. To apply a luminescent probe to biomedical imaging, one needs to assess them intracellularly and optimize the photophysical properties.

Desirable intracellular fluorescent sensors should have: (i) a signal with a high quantum yield ($\Phi$) to permit the use of glass microscope objectives, (ii) excitation wavelengths exceeding 340 nm to prevent UV-induced cell damage, (iii) emission wavelengths approaching 500 nm to avoid autofluorescence from species native to the cell and to facilitate use with typical fluorescence microscopy optical filter sets[9] and finally, (iv) sensors must have the ability to be passively and irreversibly loaded into cells. Though recently, there are significant advances in the design of fluorescent probes for $Zn^{2+}$,[10] and many of them are suitable for biological applications and have been used with some success in $Zn^{2+}$ neurobiology,[11] however, arguably all suffer from one or more limitations. For example, fluorescent $Zn^{2+}$ probe FluoZin-3, most frequently used to detect $Zn^{2+}$, has high sensitivity, quantum yield and high affinity for $Zn^{2+}$ ($K_d$ = 15 nM) at pH 7.4[12,13]) but it has a drawback in its selectivity, being fluorescent also towards $Ca^{2+}$ particularly at higher concentration.

The purpose of the present study is to design and synthesize a simple and inexpensive zinc sensor with high selectivity and sensitivity of nM range which could identify the *in vivo* and *in vitro* level of [$Zn^{2+}$] below 3 nM,[14] and at the same time would have no or negligible cytotoxicity.

Ligand **1** was prepared by simple Schiff base condensation of 4-methyl-2,6-diformylphenol(dfc) with salicylhydrazide in the presence of a catalytic amount of AcOH. The Zn-complex was prepared by the reaction of Zn-acetate and the ligand in MeCN. Single crystals suitable for X-ray diffraction were obtained by recrystallization from DMF. All these are presented in Scheme 1 and details of experimental procedures are presented in the ESI.†

Single crystal X-ray diffraction studies show that the complex **2** crystallizes in the space group $P\bar{1}$(triclinic) as a dinuclear species with a $\mu_2$-cresolato and two $\mu_2$-acetato bridge cores (Fig.1). Both Zn atoms are five-coordinated with $NO_4$ donor sets

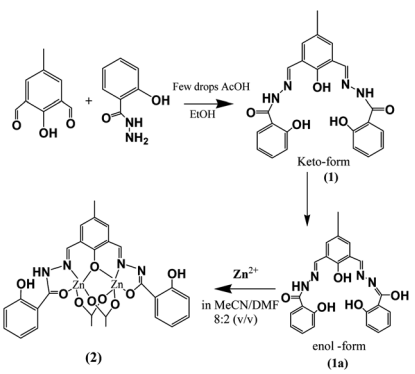


**Scheme 1**

[a]*Department of Chemistry, Jadavpur University, Kolkata 700 032, India*
[b]*Department of Botany, Kalyani University, Kalyani, 700 032, India.*
*E-mail: m_ali2062@yahoo.com*

† Electronic supplementary information (ESI) available: Details of experimental procedures. CCDC reference numbers 834115. For ESI and crystallographic data in CIF or other electronic format see DOI: 10.1039/c2ob07084g

made up of a bridging $\mu_2$-cresolato O atom, a salicylhydrazide N atom, a salicylhydrazide O atom and the other two O atoms from two different acetate ions. The O4 atom on the salicylhydrazide part is enolic type and coordinated to Zn1, while the other salicylhydrazide oxygen atom, O3 is ketonic type and coordinated to Zn2. The $\tau$ values of 0.56 [Zn1] and 0.69 [Zn2] show that the geometries at the metals are intermediate between trigonal-bipyramid and square-pyramid (for a perfect square-pyramid, $\tau = 0$ and for a perfect trigonal-bipyramid, $\tau = 1$). The separation between the two metal centers (Zn1···Zn2) is 3.182 Å. The other bond distances are O4–Zn1 = 2.0499(15), O3–Zn2 = 2.1416 (17), N5–Zn1 = 2.0256(18) and N9–Zn2 = 2.0311(18) which are the salicylhydrazide parts of the ligand. Two acetate bridges are hanging from the two penta-coordinated Zn metals. These bond distances are Zn1–O1 = 1.9751(17) Å, Zn1–O6 = 1.9802(18) Å and Zn2–O2 = 1.9633(17) Å, Zn2–O5 = 1.9554(18) Å. The two DMF (dimethyl formamide) molecules are also present in this crystal lattice with one DMF molecule showing H-bonding interaction with free –OH group, situated at *ortho*-position of salicylhydrazide with O9–H51···O11 H-bond distance = 1.83(3) Å. The selected bond angles and bond distances are listed in the Table S1.†

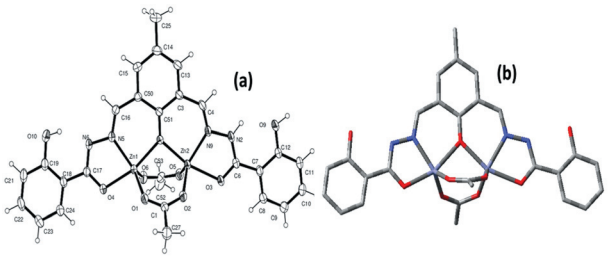


**Fig. 1** (a) ORTEP plot of compound **2** with atom numbering (30% thermal ellipsoid probability); (b) DFT optimized structure of **2**.

The spectrophotometric titration for the interaction of **1** with $Zn^{2+}$ at 25 °C in aqueous-THF buffer (HEPES buffer, pH 7.0) solution (4 : 6 v/v) reveals that there are gradual increases in absorption intensities of **1** at 434 and 350 nm and a decrease at 383 nm with isosbestic points at 390, 373 and 331 nm, accompanied by the obvious hypsochromic shift of 476 nm absorption peak of free ligand **1** to 434 nm, with the gradual increase in the concentration of $Zn^{2+}$ in the range 0–10.0 μM, keeping the concentration of **1** fixed at 10.0 μM (Fig. 2(a)).

On further increase in concentration of $Zn^{2+}$ the absorption band at 434 nm gradually shifted towards 420 nm and 383 band to 365 nm; and isosbestic points at 390 and 373 nm are shifted towards 380 and 362 nm respectively (see Fig. S5a†).This may arise due to the change in composition of **1** and $Zn^{2+}$ from 1 : 1 to 1 : 2. While the isosbestic point at 331 nm for 1 : 1 composition vanishes and a new isosbestic point is generated at 450 nm for $[Zn^{2+}] : [\mathbf{1}] > 1$. The blue shift in absorption bands of free ligand is expected to correspond to the coordination of $Zn^{2+}$ with **1** *via* nitrogen and oxygen atoms in the salicylhydrazide moiety to generate a five-membered chelate ring; which consequently extends the conjugation resulting in a shift of absorption band at 460 nm to 426 nm. The appearance of three isosbestic points also clearly indicates the transformation of **1** to the corresponding Zn-coordinated species. The composition of the complex was determined by JOB's method (inset of Fig. 2(c)) and found to be 1 : 2 with respect to ligand.

DFT calculations on complex **2** were performed using Gaussian 03 program[15] starting from the X-ray coordinates. The global minima of all these species were confirmed by the positive vibrational frequencies. The MO diagram of **2** is shown in Fig. 3. Bond distances and bond angles around the $Zn^{2+}$ centers are in agreement with the crystallographic data (see Table S1†). The UV spectrum computed from TDDFT calculations[16,17] in THF shows three important peaks in the range 270–450 nm (see inset (d) in Fig. 2). The band around 450 nm is dominated by

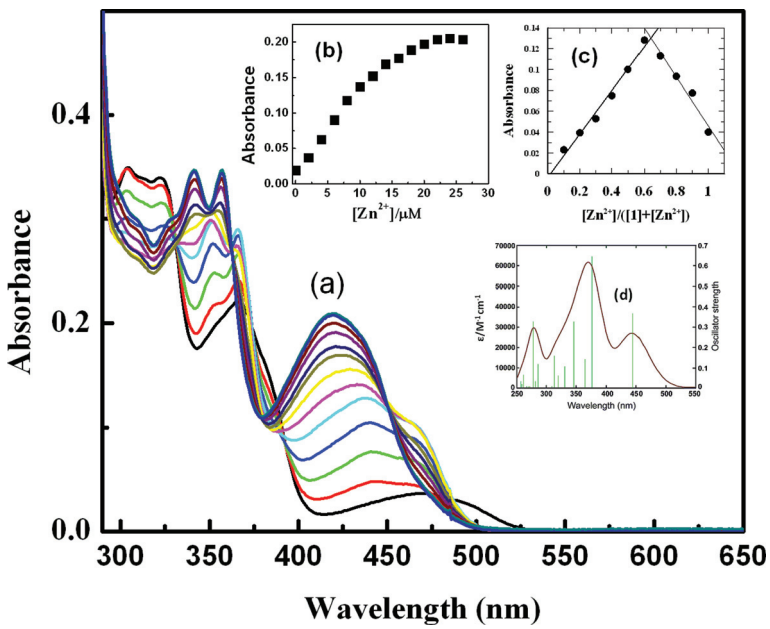


**Fig. 2** (a) Change in absorption spectra of **1** (10 μM) upon addition of $Zn^{2+}$ in HEPES buffer at pH 7.0 in $H_2O$–THF = 4 : 6 v/v at 25 °C, $[Zn^{2+}]$ = 2–30 μM. Inset (b) plot of absorbance (at 426 nm) *vs.* $[Zn^{2+}]$; (c) JOB's plot for the same reaction at 426 nm and (d) TD-DFT spectrum of 2 in THF.

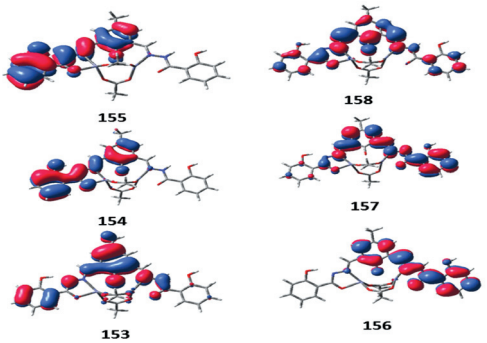


**Fig. 3** Frontier molecular orbitals of complex **2**.

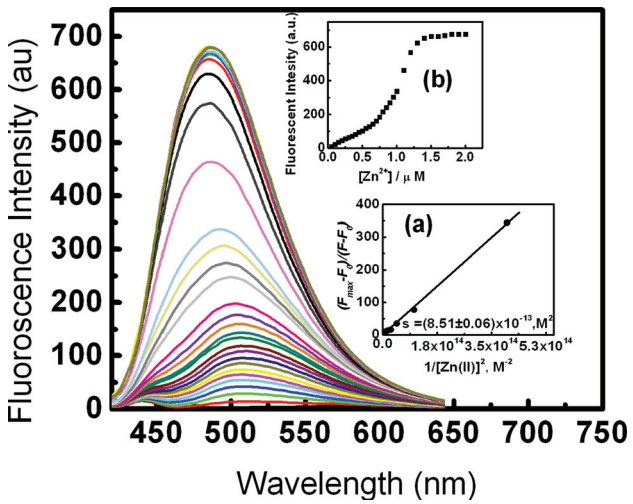


**Fig. 4** Change in fluorescence intensity ($\lambda_{ex}$ 390 nm) of **1** (1.0 μM) measured in $H_2O$–THF = 4 : 6 v/v in HEPES buffer at pH 7.0, upon addition of $Zn^{2+}$ (0–2.20 μM); Inset: (a) plot of $\{(F_{max} - F_o)/(F - F_o)\}$ *vs.* $1/[Zn^{2+}]^2$: (b) plot of F (at 490 nm) *vs.* $[Zn^{2+}]$.

the HOMO(155) → LUMO(156) excitation, while the band around 370 nm is mainly due to the HOMO(155) → LUMO + 1 (157) and HOMO − 1(154) → LUMO(156) transitions. The details of the vertical excitation energies, oscillator strengths, and nature of excitations are shown in Table S2.† The pattern of the calculated UV-Vis spectrum is very close to the experimental one.

Fig. 4 shows the change in fluorescence intensity at $\lambda_{em}$ 490 nm ($\lambda_{ex}$ 390 nm) of **1** (1.0 μM) measured in THF–water (4 : 6 v/v) with successive addition of $Zn^{2+}$ (0.05–2.2 μM) at physiological pH (7.0, HEPES buffer). The addition of $Zn^{2+}$ leads to an increase in fluorescence intensity at around 490 nm and it is saturated upon addition of 2.20 equivalent of $Zn^{2+}$. The fluorescence increase occurs immediately upon addition of $Zn^{2+}$. There is a gradual shift in $\lambda_{em}$ from 512 nm to 486 nm that may be attributed to the fact that on coordination to $Zn^{2+}$ through deprotonated cresolato and enolato oxygen atoms of the ligand leads to a decrease in the polar environment of the ligand.

As shown in Fig. 4, the fluorescence enhancement factor measured at 490 nm is determined to be ~680 at [**1**] = 1.0 μM and $[Zn^{2+}] \geq 2.0$ μM and to the best of our knowledge this seems to be the highest value among the previously reported related Zn-sensors.[10] So far the highest known fluorescence

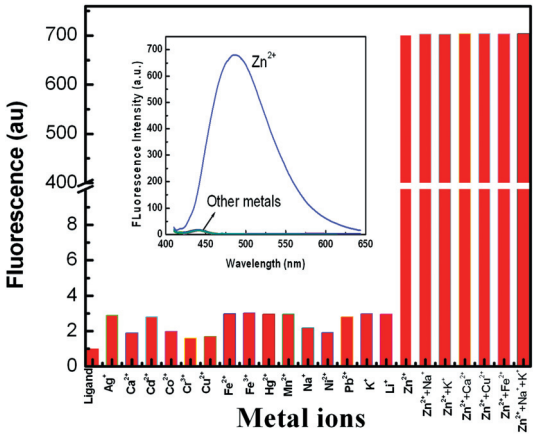


**Fig. 5** Selectivity of **1** for $Zn^{2+}$. Fluorescence response of **1** following addition of 15 equivalents of the metal ion of interest. Inset is the fluorescence spectrum of **1** in the presence of 15 equivalents of different metal ions.

enhancement is 150 times that observed in the case of ZQ1 and ZQ2[10b] In contrast, addition of other metal cations scarcely shows any fluorescence enhancement (Fig. 5).The quantum yield determination of the zinc complex gives $\Phi(2) = 0.15$, while the free ligand was found to be non- or very weakly fluorescent. The Limit of Detection (LOD) of $Zn^{2+}$ was determined by the 3σ method[18] and found to be 2.88 ng $L^{-1}$. All these findings indicate that **1** behaves as a highly sensitive fluorescent $Zn^{2+}$ sensor. Addition of TPEN (*N*,*N*,*N*′,*N*′-tetra(2-picolyl)ethylenediamine), an intracellular heavy metal ion chelator, to a solution containing **1** and $Zn^{2+}$ leads to the immediate disappearance of the yellowish-green fluorescence. This indicates that **1** reversibly coordinates to $Zn^{2+}$.

Fig. 4b shows the result of fluorescence titration of **1** with $Zn^{2+}$. There are two $Zn^{2+}$ ions coordinated to one ligand fragment and this is confirmed by the Benesi–Hildebrand method. Assuming a 1 : 2 association between **1** and $Zn^{2+}$, the Benesi–Hildebrand equation is given as:

$$\frac{(F_{max} - F_0)}{(F - F_0)} = 1 + \frac{1}{K[Zn^{2+}]^2}$$

where, $F_0$ is the fluorescence of **1** in the absence of externally added $Zn^{2+}$, $F$ is the fluorescence obtained at different $[Zn^{2+}]$ and $F_{max}$ is the fluorescence of **1** at $[Zn^{2+}]$ in large excess. $K$ ($M^{-2}$) is the association constant. As shown in Fig. 4(b), the plot of $\{(F_{max} - F_0)/(F - F_0)\}$ *vs.* $1/[Zn^{2+}]^2$ yields a straight line with slope = (8.51 ± 0.06) × $10^{-13}$, indicating that **1** indeed associates with $Zn^{2+}$ in a 1 : 2 stoichiometry. The intercept value 1.07 ± 0.48, close to 1.0, also manifests the self-consistency of the experimental data. Therefore, the ligand dissociation constant $K_d$ is ~0.85 $pM^2$. The 1 : 2 complex formation in solution is further confirmed by ESI-$MS^+$-($m/z$) analysis with a peak at 887.65 that corresponds to the composition $\{[Zn_2(\mathbf{1})(CH_3COO)_2]\cdot(NMe_2CHO)_2\ CH_3CN + Na^+\}$.

Zinc detection was not perturbed by biologically abundant $Li^+$, $Na^+$, $K^+$, $Mg^{2+}$, $Ca^{2+}$ *etc.* metal ions. Several transition metals, namely $Cr^{3+}$, $Mn^{2+}$, $Fe^{2+}$, $Fe^{3+}$, $Co^{2+}$, $Ni^{2+}$, $Cu^{2+}$, $Cd^{2+}$, $Pb^{2+}$, and $Hg^{2+}$, also caused no interference (Fig. 5).

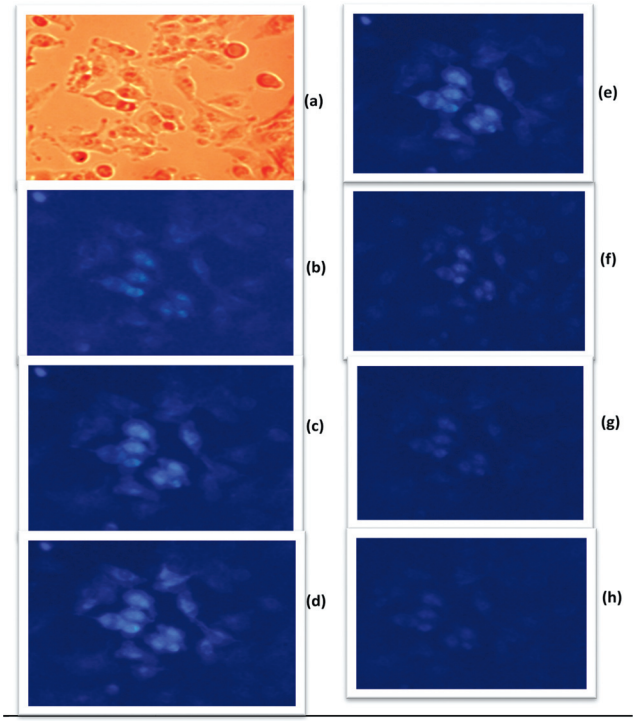


**Fig. 6** Fluorescence microscopic observations: (a) Phase contrast and (b) fluorescence images of A375 cells induced by intracellular $Zn^{2+}$ when incubated with 10 μM zinc sensor for 30 min at 37 °C and washed with PBS. Cells were exposed to sequentially increasing concentrations of added extracellular $Zn^{2+}$ as (c) 10 μM, (d) 20 μM and (e) 30 μM. The return of intracellular $Zn^{2+}$ to the resting level (f–h) was achieved by the addition of zinc sensor inhibitor (TEPN, 100 μM), at 5 min interval. For all imaging, the samples were excited at ~360 nm.

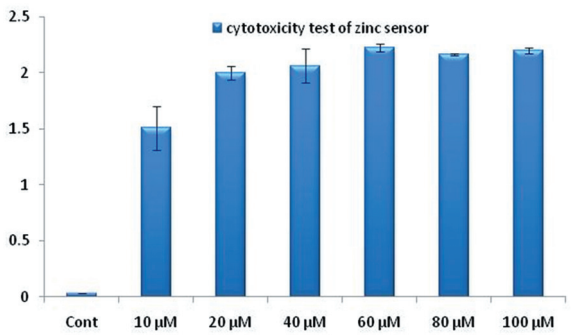


**Fig. 7** Cytotoxicity assay of zinc sensor: Histogram represents the cytotoxicity of zinc sensor on A375 cells at various concentrations, after 2 h of incubation. The cell cytotoxicity was calculated as % cell cytotoxicity = 100% − % cell viability.

Furthermore, the emission profile and zinc response of **1** are stable at physiological pH ~7.0, therefore this probe does not suffer from a common weakness of other reported *in vivo* probes.

The intracellular $Zn^{2+}$ imaging behavior of zinc sensor **1** was initially studied on A375 human melanoma cancer cells by fluorescence microscopy. After incubation with the zinc sensor (10 μM in 0.01 M HEPES buffer, pH 7.0) at 37 °C for 10 min, the cells displayed intracellular fluorescence (Fig. 6b), indicating the ability of the probe to sense $Zn^{2+}$ inside the cell of intracellular concentration (~3 ng $L^{-1}$). The cells also exhibited more intense fluorescence when $Zn^{2+}$ was introduced onto the cells externally, and fluorescence responses increase with the increase in $Zn^{2+}$ concentration, which could be evident from the cellular imaging (Fig. 6c–e). However, the fluorescence of the cells was deeply suppressed when the inhibitor, TPEN, of the $Zn^{2+}$ sensor was added onto the cells (Fig. 6f–h). These observations clearly indicate that the present zinc sensor is an efficient candidate for monitoring changes in the intracellular $Zn^{2+}$ concentration under biological conditions. Fluorescence intensities of cells of different experimental groups were analyzed and have been additionally incorporated as Fig. S10.†

In order to test the cytotoxicity of **1** on the cell, we also performed MTT assay[19] in A375 human melanoma cancer cells treated with various concentrations of zinc sensor for up to 2 h (Fig. 7). But the result showed no significant cell death in 2 h incubation of **1** up to 100 μM. This would therefore suggest that this zinc sensor can readily be used for cellular application at the indicated dose and time of incubation without worry about its cytotoxicity.

To confirm our findings, we also subjected HeLa cells (a human cervical carcinoma cell line) to the same type of treatments and the results we obtained were essentially similar in nature. Therefore, its use in biological materials as an effective zinc monitoring candidate was further confirmed.

In summary, we have developed a simple and inexpensive zinc sensor that features visible excitation and emission profiles, excellent selectivity responses for $Zn^{2+}$ over other competing physiological metal ions at intracellular concentrations, a dissociation constant $K_d$ < 1 $pM^2$, and a ~680-fold increase in fluorescence emission intensity upon zinc binding leading to LOD ~1 nM without requiring microinjection for intracellular use.

## Acknowledgements

Financial support from CSIR (Ref No. 01(2490)/11/EMR-II) and DST (Ref. SR/S1/IC-35/2006), New Delhi, India are gratefully acknowledged. T.M. acknowledges the fellowship from UGC (UGC-NET).

## References

1 C. J. Frederickson, Neurobiology of zinc and zinc-containing neurons, *Int. Rev. Neurobiol.*, 1989, **31**, 145.
2 C. J. Frederickson, M. A. Klitenick, W. I. Manton and J. B. Kirkpatrick, *Brain Res.*, 1983, **273**, 335.
3 J. Perez-Clausell and G. Danscher, *Brain Res.*, 1985, **337**, 91.
4 (*a*) N. L. Harrison and S. J. Gibbons, *Neuropharmacology*, 1994, **33**, 935; (*b*) T. G. Smart, X. Xie and B. J. Krishek, *Prog. Neurobiol.*, 1994, **42**, 393.
5 (*a*) G. L. Westbrook and M. L. Mayer, *Nature*, 1987, **328**, 640; (*b*) S. Peters, J. Y. Koh and D. W. Choi, *Science*, 1987, **236**, 589.
6 N. Tonder, F. F. Johansen, C. J. Frederickson, J. Zimmer and N. H. Diemer, *Neurosci. Lett.*, 1990, **109**, 247.
7 R. S. Sloviter, *Brain Res.*, 1985, **330**, 150.
8 Y. Y. Long, S. W. Suh, N. F. M. S. Pons, J. W. Jensen, M. Chen, G. Motamedi, G. Danscher and C. J. Frederickson, *Soc. Neurosci. Abstr.*, 1998, **24**, 1727.
9 A. W. Czarnik, *Curr. Biol.*, 1995, **2**, 423.
10 (*a*) K. Komatsu, K. Kikuchi, H. Kojima, Y. Urano and T. Nagano, *J. Am. Chem. Soc.*, 2005, **127**, 10197; (*b*) E. M. Nolan, J. Jaworski, K.-I. Okamoto, Y. Hayashi, M. Sheng and S. J. Lippard, *J. Am. Chem. Soc.*,

2005, **127**, 16812; (*c*) P. Roy, K. Dhara, M. Manassero, J. Ratha and P. Banerjee, *Inorg. Chem.*, 2007, **46**, 6405; (*d*) Y. Mikata, M. Wakamatsu, A. Kawamura, N. Yamanaka, S. Yano, A. Odani, K. Morihiro and S. Tamotsu, *Inorg. Chem.*, 2006, **45**, 9262; (*e*) E. M. Nolan, J. Jaworski, M. E. Racine, M. Sheng and S. J. Lippard, *Inorg. Chem.*, 2006, **45**, 9748; (*f*) N. C. Lim, J. V. Schuster, M. C. Porto, M. A. Tanundra, L. Yao, H. C. Freake and C. Brckner, *Inorg. Chem.*, 2005, **44**, 2018; (*g*) E. M. Nolan and S. J. Lippard, *Inorg. Chem.*, 2004, **43**, 8310; (*h*) E. M. Nolan, S. C. Burdette, J. H. Harvey, S. A. Hilderbrand and S. J. Lippard, *Inorg. Chem.*, 2004, **43**, 2624; (*i*) K. Komatsu, Y. Urano, H. Kojima and T. Nagano, *J. Am. Chem. Soc.*, 2007, **129**, 13447; (*j*) K. R. Gee, Z.-L. Zhou, W.-J. Qian and R. Kennedy, *J. Am. Chem. Soc.*, 2002, **124**, 776; (*k*) S. C. Burdette, G. K. Walkup, B. Spingler, R. Y. Tsien and S. J. Lippard, *J. Am. Chem. Soc.*, 2001, **123**, 7831; (*l*) H. A Godwin and J. M. Berg, *J. Am. Chem. Soc.*, 1996, **118**, 6514; (*m*) Y. Liu, N. Zhang, Y. Chen and L. H. Wang, *Org. Lett.*, 2007, **9**, 315; (*n*) E. Tomat and S. J. Lippard, *Inorg. Chem.*, 2010, **49**, 9113; (*o*) Y.-M. Li, J. Shi, X. Wu, Z.-F. Luo, F.-L. Wang and Q.-X. Guo, *Cell Biochem. Funct.*, 2009, **27**, 417; (*p*) Z. Xu, K.-H. Baek, H. N. Kim, J. Cui, X. Qian, D. R. Spring, I. Shin and J. V. Yoon, *J. Am. Chem. Soc.*, 2010, **132**, 601; (*q*) A. R. Lippert, E. J. New and C. J. Chang, *J. Am. Chem. Soc.*, 2011, **133**, 10078; (*r*) K. Komatsu, Y. Urano, H. Kojima and T. Nagano, *J. Am. Chem. Soc.*, 2007, **129**, 1344; (*s*) G.-C. Kuang, J. R. Allen, M. A. Baird, B. T. Nguyen, L. Zhang, T. J. Morgan Jr, C. W. Levenson, M. W. Davidson and L. Zhu, *Inorg. Chem.*, 2011, **50**, 10493; (*t*) L. M. T. Canzoniero, D. M. Turetsky and D. W. Choi, *J. Neurosci.*, 1999, **19** RC31, 1.

11 (*a*) B. L. Vallee and K. H. Falchuk, *Psychol. Rep.*, 1993, **73**, 79; (*b*) C. J. Frederickson and D. W. Moncrieff, *Biol. Signals*, 1994, **3**, 127; (*c*) A. Takeda, *BioMetals*, 2001, **14**, 343; (*d*) S. Dubben, A. Hönscheid, K. Winkler, L. Rink and H. Haas, *J. Leukocyte Biol.*, 2010, **87**, 833 and the references therein; (*e*) C. J. Chang, J. Jaworski, E. M. Nolan, M. Sheng and S. J. Lippard, *Proc. Natl. Acad. Sci. U. S. A.*, 2004, **101**, 1129; (*f*) P. Babula, V. Kohoutkova, R. Opatrilova, I. Dankova, M. Masarik and R. Kizek, *Chim. Oggi-Chem. Today*, 2010, **28**, 18.

12 (*a*) A. R. Kay and J. Neur, *Science*, 2003, **23**, 6847; (*b*) J. Zhao, B. A. Bertoglio, K. R. Gee and A. R. Kay, *Cell Calcium*, 2008, **44**, 422; (*c*) R. P. Haugland, *Handbook of Fluorescent Probes and Research Products*, Molecular Probes, Inc., Eugene, OR, 8th edn, 2001; Y.-M. Li, J. Shi, X. Wu, Z.-F. Luo, F.-L. Wang and Q.-X. Guo, *Cell Biochem. Funct.*, 2009, **27**, 417.

13 (*a*) G. K. Walkup, S. C. Burdette, S. J. Lippard and R. Y. Tsien, *J. Am. Chem. Soc.*, 2000, **122**, 5644; (*b*) S. C. Burdette, G. K. Walkup, B. Spingler, R. Y. Tsien and S. J. Lippard, *J. Am. Chem. Soc.*, 2001, **123**, 7831; (*c*) S. C. Burdette, C. J. Frederickson, W. M. Bu and S. J. Lippard, *J. Am. Chem. Soc.*, 2003, **125**, 1778; (*d*) E. M. Nolan, S. C. Burdette, J. H. Harvey, S. A. Hilderbrand and S. J. Lippard, *Inorg. Chem.*, 2004, **43**, 2624; (*e*) C. J. Chang, E. M. Nolan, J. Jaworski, S. C. Burdette, M. Sheng and S. J. Lippard, *Chem. Biol.*, 2004, **11**, 203; (*f*) C. J. Chang, E. M. Nolan, J. Jaworski, K. I. Okamoto, Y. Hayashi, M. Sheng and S. J. Lippard, *Inorg. Chem.*, 2004, **43**, 6774.

14 (*a*) K. R. Gee, Z. L. Zhou, D. Ton-That, S. L. Sensi and J. H. Weiss, *Cell Calcium*, 2002, **31**, 245; (*b*) K. R. Gee, Z. L. Zhou, W. J. Qian and R. Kennedy, *J. Am. Chem. Soc.*, 2002, **124**, 776.

15 M. J. Frisch *et al.*, *Gaussian 03, revision C.02*, Gaussian, Inc., Wallingford, CT, 2004..

16 P. J. Hay and W. R. Wadt, *J. Chem. Phys.*, 1985, **82**, 299.

17 (*a*) S. Miertus, E. Scrocco and J. Tomasi, *Chem. Phys.*, 1981, **55**, 117; (*b*) V. Barone, M. Cossi and J. Tomasi, *J. Comput. Chem.*, 1998, **19**, 404.

18 V. Thomsen, D. Schatzlein and D. Mercuro, *Spectroscopy*, 2003, **18**, 112.

19 J. Ratha, K. A. Majumdar, S. K. Mandal, R. Bera, C. Sarkar, B. Saha, C. Mandal, K. D. Saha and R. Bhadra, *Mol. Cell. Biochem.*, 2006, **290**, 113.



 